Supporting Information

Instrumentation.

UV-vis spectra were recorded on a PerkinElmer UV/vis spectrometer. Infrared spectra were recorded in the range of 4000-400 cm^{-1} on a Vertex 70 Bruker spectrophotometer on KBr pellets. ^1H NMR spectra were recorded on a JEOL 500 MHz instrument. The residual ^1H resonances of the solvents were used as a secondary reference. Elemental (C, H, and N) analyses were performed on a PerkinElmer 2400II elemental analyzer.

X-ray Structure Solution and Refinement.

Single-crystal X-ray data were collected at 100 K on a Bruker SMART APEX CCD diffractometer equipped with CRYO Industries low temperature apparatus and intensity data were collected using graphite-monochromated Mo Kα radiation (λ= 0.71073 Å). The data integration and reduction were processed with SAINT software.[1] An absorption correction was applied.[2] The structure was solved by the direct method using SHELXS-97 and was refined on F2 by full-matrix least-squares technique using the SHELXL-2018 program package.[3] Non-hydrogen atoms were refined anisotropically. In the refinement, hydrogen was treated as riding atoms using SHELXL default parameters.

Computational Details.

All the calculations in the work were implemented by using Gaussian 09, revision B.01 suit of programs.[4] The molecular structures of *U*-[*trans*-**2**]$(SbCl_6)_2$ and *P*'-[*trans*-**3**]$(SbCl_4)_2$•$2SbCl_3$ were optimized using the uB3LYP functional with the cc-pVQZ basis set for Nickel atom, LANL2DZ for Sb atom and 6-31G+(d,p) for all other atoms. Harmonic vibrational frequency analysis was carried out to ensure that the optimized structures were true minima without imaginary frequencies on the potential energy surface. Single point energy calculations at the uB3LYP level of theory were performed from the crystal structure coordinates for calculating the interaction energy (ΔE_{int}) in *U*-[*trans*-**2**]$(SbCl_6)_2$ and *P*'-[*trans*-**3**]$(SbCl_4)_2$•$2SbCl_3$. This method used was Becke's three-parameter hybrid-exchange functional,[5] the non-local correlation provided by the Lee, Yang, and Parr expression, and the Vosko, Wilk, and Nuair 1980 correlation functional (III)

for local correction.[6] The interaction energy (ΔE_{int}) is the energy difference between the total energy of the complex and sum of total energies of its constituent anions. The molecular electrostatic potential map was also plotted to analyze the molecular electronic properties, which can be used to understand the non-covalent interactions. All the TD-DFT calculations were performed at the CAM-B3LYP[7] level.

Moreover, to understand the specific interaction in the *U*-[*trans*-**2**]$(SbCl_6)_2$ and *P*'-[*trans*-**3**]$(SbCl_4)_2$•$2SbCl_3$, quantum theory of Atoms in Molecules (QTAIM) were employed. QTAIM can be used to analyze the bond critical points (BCPs) and cage critical points (CCPs) forming in the various kind of non-covalent interactions. The topology characteristics of the critical points (CPs) were estimated using DAMQT 2.1 software.[8] The wave functions obtained at the CAM-B3LYP level of theory have been analyzed using the program "Multiwfn -- A Multifunctional Wavefunction Analyzer" (version 3.5).[9] Visualization of the molecular orbitals and the corresponding diagrams were done using the Chemcraft software.[10]

Experimental Section:

Materials:

The *trans*-1,2-bis(meso-octaethylporphyrinyl)ethene Ni(II), *trans*-**1** and *cis*-1,2-bis(meso-octaethylporphyrinyl)ethene Ni(II), *cis*-**1** have been synthesized according to the procedures reported in the literature.[11] Reagents and solvents are purchased from commercial sources and purified by standard procedures before use. Reagents and solvents were purchased from commercial sources and purified by standard procedures before use.

Synthesis of *U*-[*trans*-**2**]$(SbCl_6)_2$**:**

To a dichloromethane (25 mL) solution of *trans*-**1**/*cis*-**1** (100 mg, 0.082 mmol), a solution of 135 mg (0.164 mmol) Tris(4-bromophenyl)ammoniumyl hexachloroantimonate in 2 mL CH_3CN was added and the resulting solution was stirred in air at room temperature for 30 minutes. During the progress of the reaction, the colour of the solution changed from red to violet and filtered through a small plug of silica gel with copious washings (CH_2Cl_2). The solution was then evaporated to complete dryness. The resulting solid was then dissolved in a minimum volume of CH_2Cl_2, filtered off to remove unreacted oxidant and then carefully layered with n-hexane. On standing for 6-7 days in air at room temperature, dark red needle crystals were

obtained, which was then isolated by filtration, washed well with n-hexane, and dried in vacuum. Yield: 110 mg (70%). UV-vis (chloroform) [λ_{max}, nm (ε, M^{-1} cm^{-1})]: 404 (3.1×10^5), 514 (2.1×10^5), 958 (2.6×10^5); ESI-MS: m/z 1539.3053 for {*U*-[*trans*-**2**]$(SbCl_6)_2$−$SbCl_6$}$^+$; Elemental analysis (%) calcd (found) for $C_{76}H_{92}Cl_{16}N_8Ni_2Sb_2$: C, 44.62 (44.83); H, 4.53 (4.72); N, 5.48 (5.31). ^{1}H NMR ($CDCl_3$, 295 K): (−C*H* (b)), 3.48 (meso-*H*), 2.16, and 1.99; (ethyl −CH_2) 1.55 and (−CH_3) 1.32, 1.29, 1.27, 1.24, 1.14, 1.10, 1.03, 0.96, 0.95, 0.88, 0.87, 0.86, 0.84, 0.83, 0.82 and 0.81 ppm.

Synthesis of *P*'-[*trans*-**3**]$(SbCl_4)_2$•2$SbCl_3$:

trans-**1**/*cis*-**1** (100 mg, 0.082 mmol) was dissolved in CH_2Cl_2 (25 mL) and a solution of 203 mg (0.246 mmol) tris(4-bromophenyl)ammoniumyl hexachloroantimonate in 2 mL CH_3CN was added to it or in *U*-[*trans*-**2**]$(SbCl_6)_2$ (100 mg, 0.083 mmol) was dissolved in CH_2Cl_2 (25 mL) and a solution of 67.83 mg (0.083 mmol) tris(4-bromophenyl)ammoniumyl hexachloroantimonate in 2 mL CH_3CN was added to it. The solution was stirred in air at room temperature for 30 minutes. During the progress of the reaction, the colour of the solution has changed from light violet to dark violet and filtered through a small pack of silica gel with copious washings (CH_2Cl_2). The resulting solution was then evaporated to complete dryness. The solid thus obtained was dissolved in a minimum volume of CH_2Cl_2, filtered off to remove unreacted oxidant and then carefully layered with n-hexane. On standing for 8-10 days in air at room temperature, dark red crystals were obtained. The crystalline solid was then isolated by filtration, washed well with n-hexane, and dried in vacuum. Yield: 115 mg (64%). UV-vis (chloroform) [λ_{max}, nm (ε, M^{-1} cm^{-1})]: 391 (2.1×10^5), 510 (2.0×10^5), 710 (1.3×10^5), 1600(8.6×10^4); ESI-MS: m/z 604.2994 for {*P*'-[*trans*-**3**]}$^{2+}$; Elemental analysis (%) calcd (found) for $C_{76}H_{92}Cl_{18}N_8Ni_2Sb_4$: Anal. Calcd (found): C, 38.68 (38.91); H, 3.93 (4.14); N, 4.75 (4.91). ^{1}H NMR ($CDCl_3$, 295 K): (−C*H* (b)), 5.29 (meso-*H*), 3.47, and 2.16; (ethyl −CH_2) 1.87, and 1.57 (−CH_3) 1.32, 1.28, 1.25, 1.10, 1.05 0.98, 0.97, 0.92, 0.90, 0.88, 0.84, 0.81, 0.80, and 0.68ppm.

References:

1. SAINT+, 6.02 ed., Bruker AXS, Madison, WI, **1999**.

2. Sheldrick, G. M.; SADABS 2.0, **2000**.

3. Sheldrick, G. M. SHELXL-2018: Program for Crystal Structure Refinement; University of Göttingen: Göttingen, Germany, 2018.

4. Frisch, M. J. T.; Trucks, G. W.; Schlegel, H. B.;Scuseria, G. E.; Robb, M. A. C.;Cheeseman,J. R.; Scalmani, G.; Barone, V.; Mennucci, G. A. N. B.; Petersson, H.; Caricato, M.; Li, X. ; Hratchian, H. ; Izmaylov, A. F.; Bloino, J.; Zheng, G.; Sonnenberg, J. L.; Hada, M.; Ehara, M.;Toyota, K.; Fukuda, R.; Hasegawa, J.; Ishida, M.; Nakajima, Y. K. T.; Honda, O.; Nakai, H. ;Vreven, T.; Montgomery, J. A.; Peralta, Jr. J. E. O. ; Oligaro, F.; Bearpark, M.; Heyd, J. J.; rothers, E.; Kudin, V. N.; Staroverov, K. K. N. R.; Normand, J.;Raghavachari, K.; Rendell, A. B.; Iyengar, S. S.; Tomasi, J.; Cossi, M.; Rega, J. M.; Millam, M.; Knox, J. E.; Cross, J. B.; Bakken, V.; Adamo, C. J.; Gomperts, J.; Stratmann, R. E.; Yazyev, O.; Austin, A. J.; Cammi, R.;Pomelli, J. W.; Ochterski, J. W.; Martin, R. L.; Morokuma, K. Z.; Zarkrzewski, V. G.; Voth, G. A.; Salvador, P.; Dannenberg, J. J. D.; Dapprich, S.; Daniels, A. D.; Farkas, ö.; Foresman, J. B.; Ortiz, J. V.; Cioslowski, J.; Fox, D. J. *Gaussian 09, Revision B.01*, Gaussian, Inc., Wallingford, CT, **2010**.

5. A. D. Becke, *J. Chem. Phys.***1993**, *98,* 5648.

6. C. Lee, W. Yang and R. G. Parr, *Phys. Rev. B.* **1988**, *37*, 785.

7. T. Yanai, D. P. Tew and N. C. Handy, *Chem. Phys. Lett.*, **2004**, *393*, 51.

8. (a) R. López, J. F. Rico, G. Ramírez, I. Ema, D. Zorrilla, A. Kumar, S. D. Yeole, S. R. Gadre, *Comput. Phys. Commun*. **2017**, *214*, 207; (b) A. Kumar, S. D. Yeole, S. R. Gadre, R. López, J. F. Rico, G. Ramírez, I. Ema, D. Zorrilla, *J. Comput. Chem*. **2015**, *36*, 2350.

9. T. Lu, F. Chen, *J. Comput. Chem.* **2012**, *33*, 580.

10. http://www.chemcraftprog.com.

11. T. E. Clement, D. J. Nurco, K. M. Smith, *Inorg. Chem*. **1998**, 37, 1150.

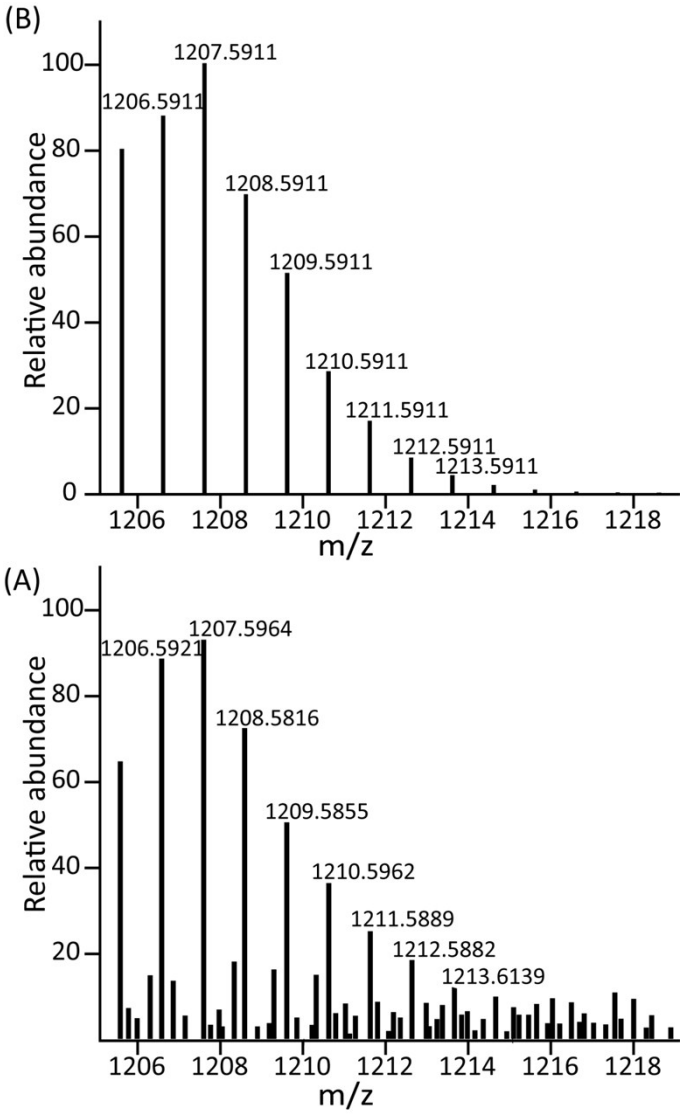

Fig. S1. Isotopic distribution pattern of the (A) experimental and (B) simulated ESI-MS spectrum (positive ion mode) of *trans*-**1.** Spectrum shows a molecular ion peak at m/z 1207.5964 corresponding to [*trans*-**1**]$^{+}$.

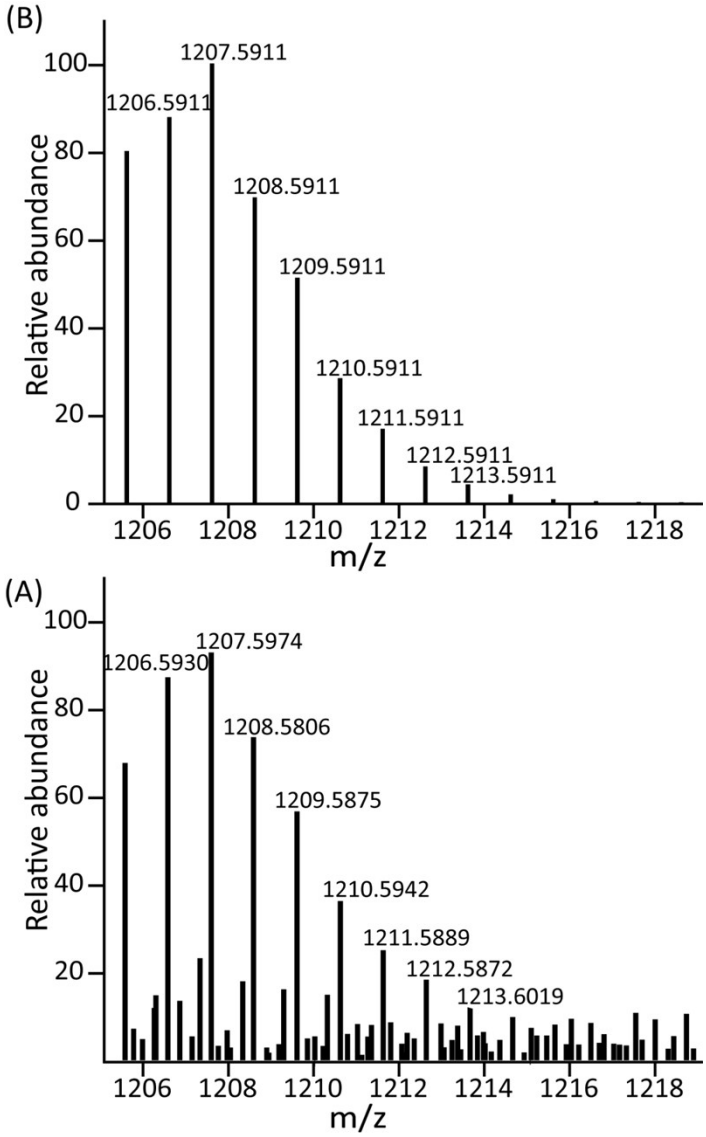

Fig. S2. Isotopic distribution pattern of the (A) experimental and (B) simulated ESI-MS spectrum (positive ion mode) of *cis*-**1.** Spectrum shows a molecular ion peak at m/z 1207.5974 corresponding to [*cis*-**1**]$^{+}$.

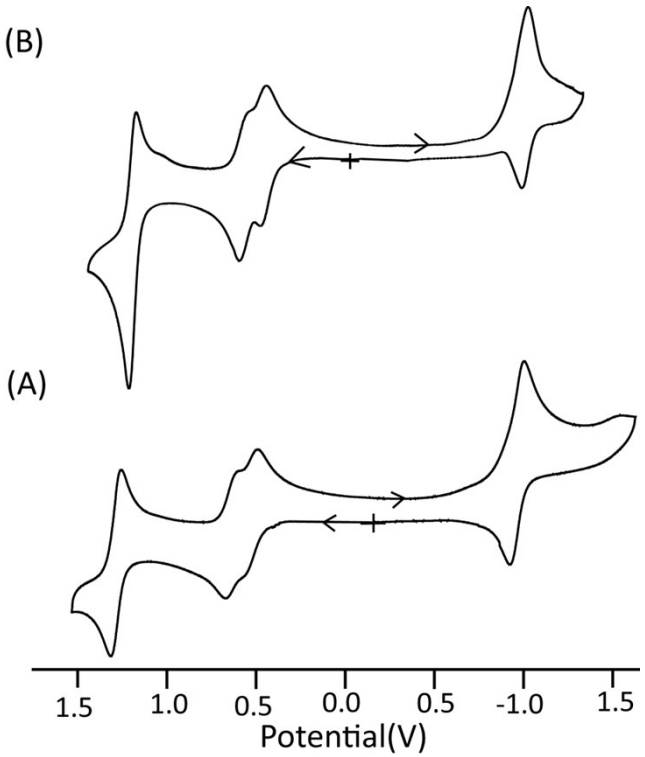

Fig. S3. Cyclic voltammogram (at 295 K in CH_2Cl_2) of (A) *trans*-**1** and (B) *cis*-**1** (scan rate = 100 mV/s) with 0.1 (M) tetra(n-butyl)ammoniumhexafluorophosphate as a supporting electrolyte. The reference electrode was Ag/AgCl.

Table S1. Electrochemical data (in dichloromethane at 298 K) for complexes *trans*-**1** and *cis*-**1**.

Complexes	Oxidation			Reduction
	E_{ox} (I) [V (mV)]	E_{ox} (II) [V (mV)]	E_{ox} (III) [V (mV)]	E_{red} (I) [V]
trans-**1**	0.53(60)	0.61(65)	1.29(75)	-0.96
cis-**1**	0.54(65)	0.62(70)	1.25(65)	-0.95

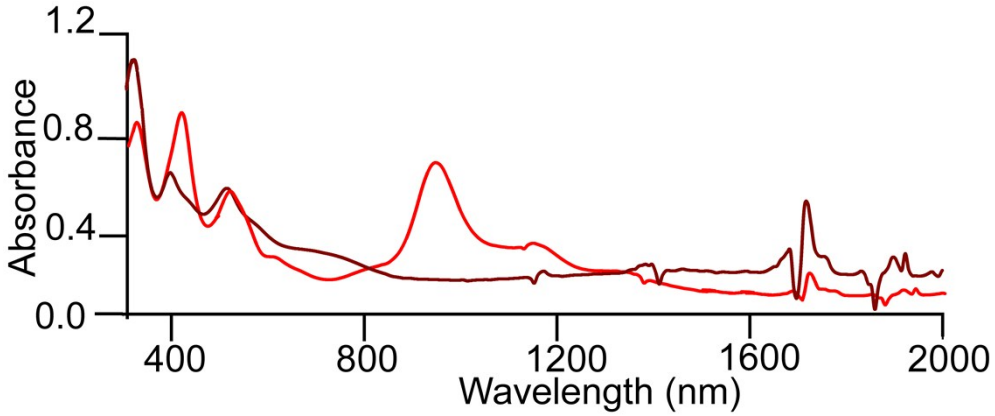

Fig. S4. UV-visible spectra (in $CHCl_3$ at 295 K) using polycrystalline samples of *U*-[*trans*-**2**]$(SbCl_6)_2$ (red line) and *P*'-[*trans*-**3**]$(SbCl_4)_2$•$2SbCl_3$ (brown line).

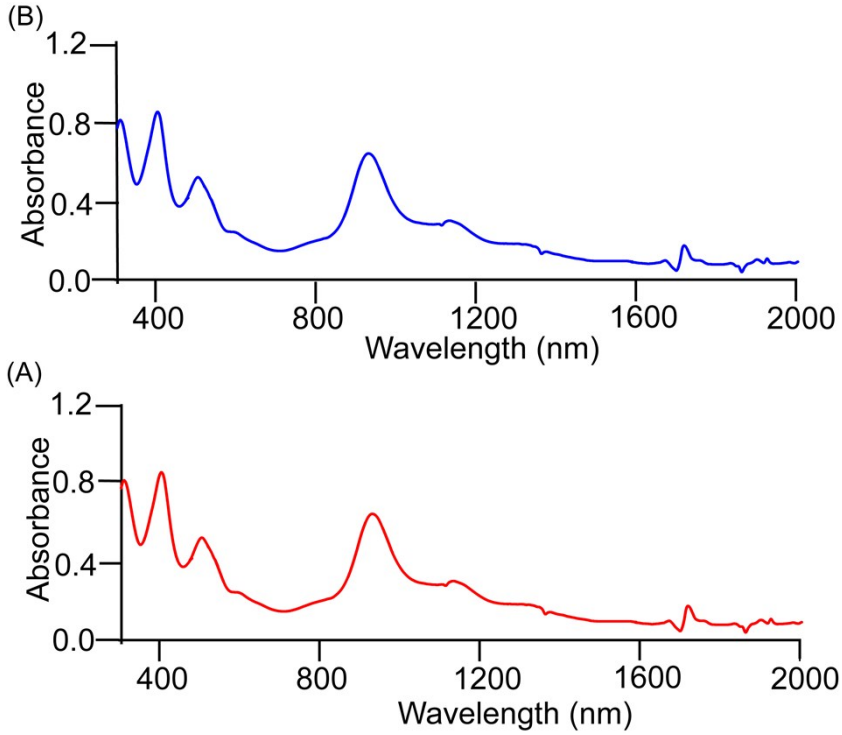

Fig. S5. UV-vis-NIR spectra (in $CHCl_3$ at 295 K) of *U*-[*trans*-**2**]$(SbCl_6)_2$ after refluxing the solution under nitrogen for (A) 1 hr and (B) 12 hrs with excess of tetra(n-butyl)ammoniumhexafluorophosphate.

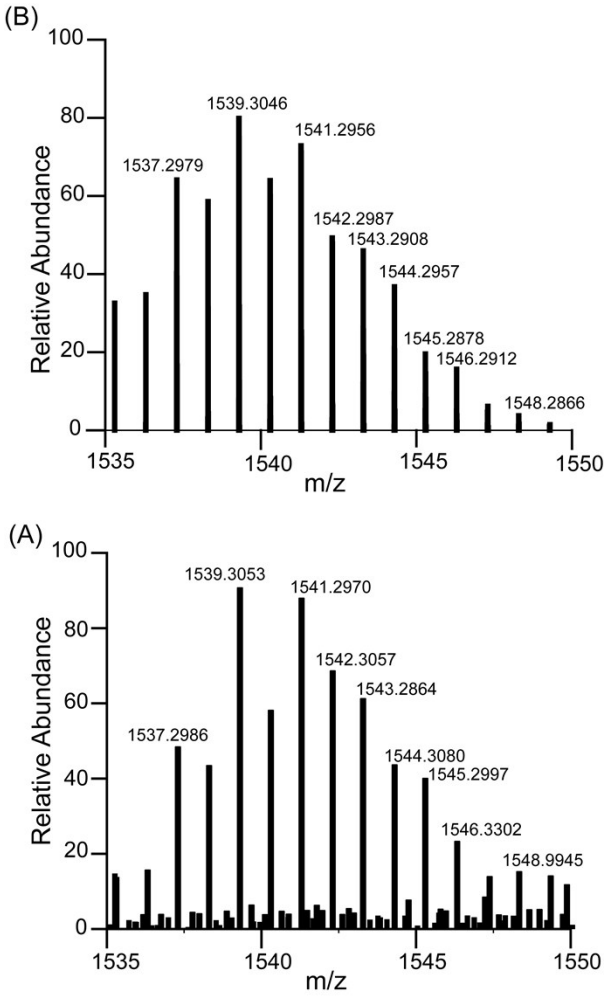

Fig. S6. Isotopic distribution pattern of (A) experimental and (B) simulated ESI-MS spectrum (positive ion mode) of *U*-[*trans*-**2**]$(SbCl_6)_2$. Spectrum shows a molecular ion peak at m/z 1539.3053 corresponding to $\{U\text{-}[trans\text{-}\mathbf{2}](SbCl_6)_2 - SbCl_6\}^+$.

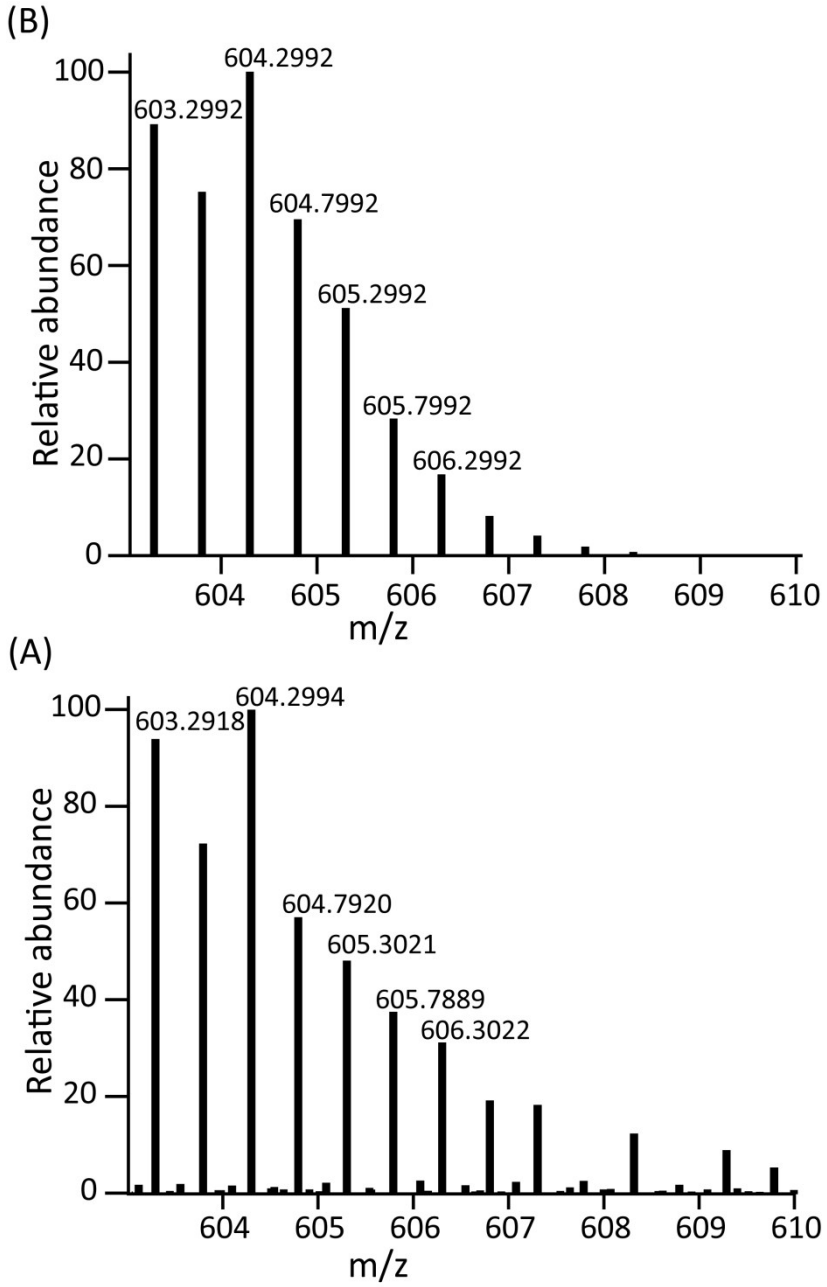

Fig. S7. Isotopic distribution pattern of the (A) experimental and (B) simulated ESI-MS spectrum of *P*'-[*trans*-**3**]$(SbCl_4)_2$•$2SbCl_3$. Spectrum shows a molecular ion peak at m/z 604.2994 for $\{$*P*'-[*trans*-**3**]$\}^{2+}$

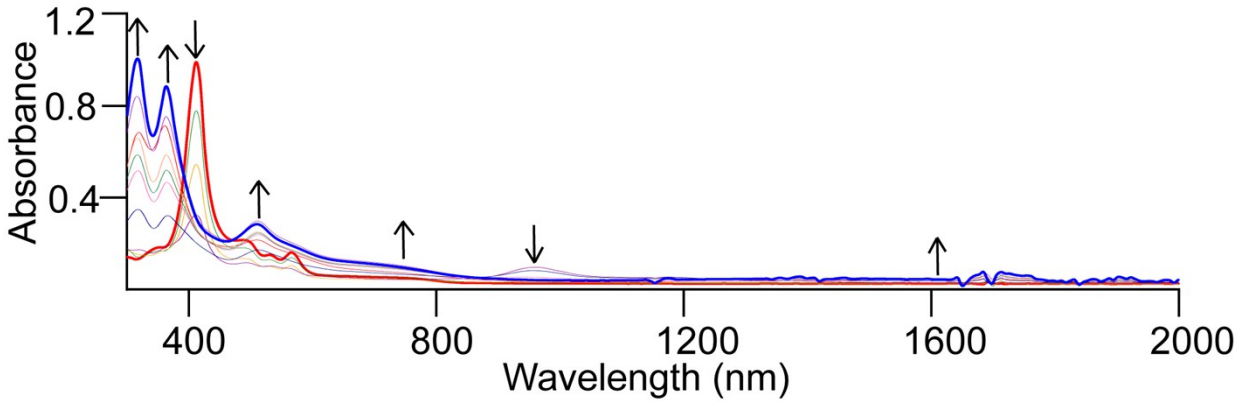

Fig. S8. UV-vis-NIR spectral change (in CH_2Cl_2 at 298 K) of 1.2 x 10^{-5} (M) solution of *trans*-**1** (red line) upon gradual additions of 0 to 3.5 eq. of. $FeCl_3$.

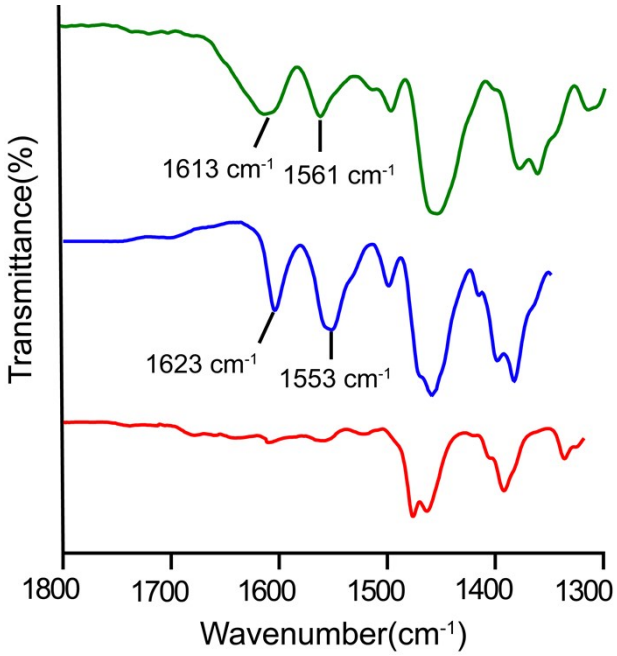

Fig. S9. IR spectra (selected portions only) of solid polycrystalline samples of *trans*-**1** (red line), (B) *U*-[*trans*-**2**]$(SbCl_6)_2$ (blue-line) and (C) *P*'-[*trans*-**3**]$(SbCl_4)_2$•$2SbCl_3$ (green-line). The marker bands related to π-cation radicals are labeled.

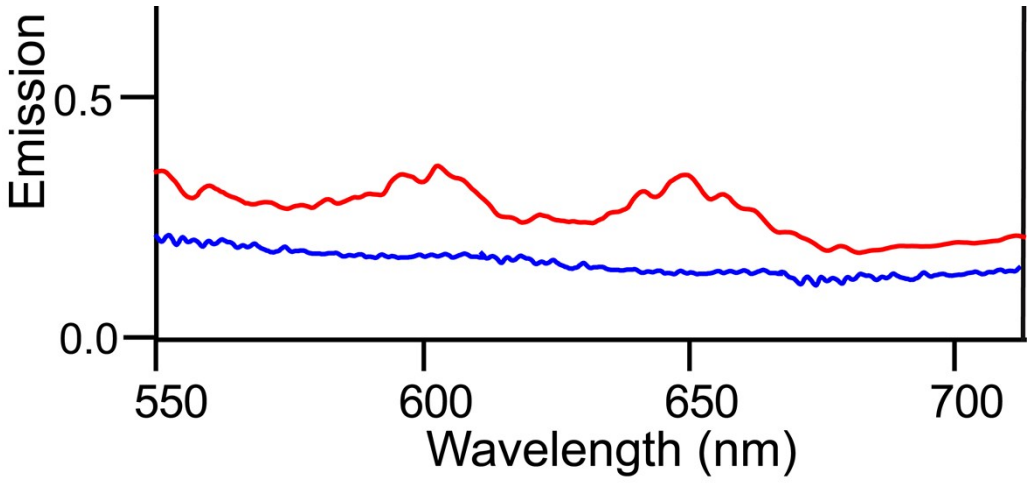

Fig. S10. Normalized emission spectra of *U*-[*trans*-**2**]$(SbCl_6)_2$ (red colour) and *P*'-[*trans*-**3**]$(SbCl_4)_2$•$2SbCl_3$ (blue colour) excited at 420 nm in chloroform at 295 K.

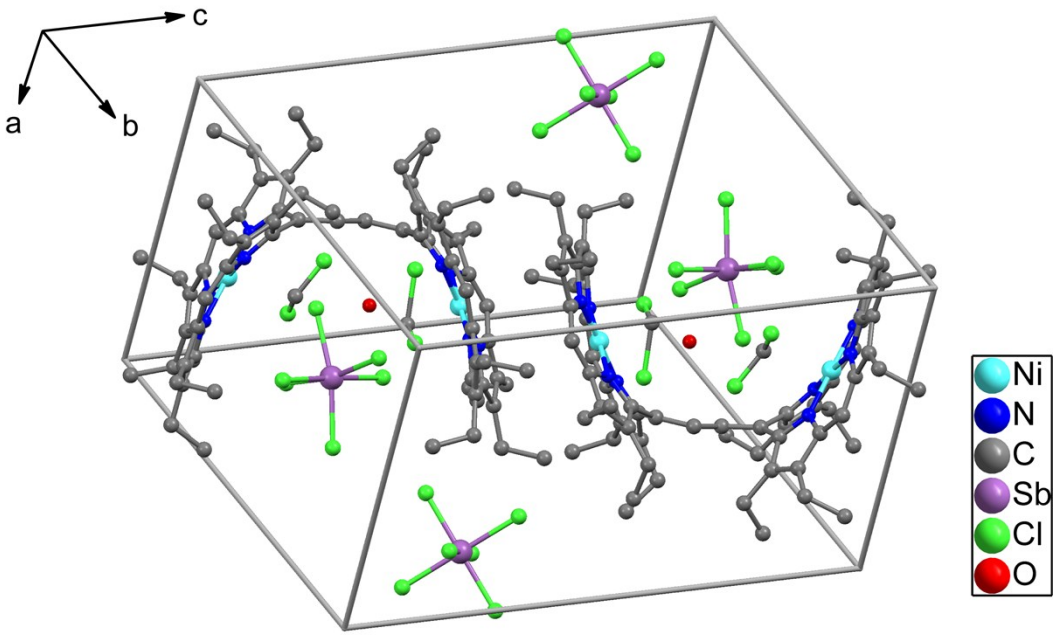

Fig. S11. Diagram illustrating the molecular packing of *U*-[*trans*-**2**]$(SbCl_6)_2 \bullet 2CH_2Cl_2 \bullet H_2O$ in the unit cell (H atoms and solvent molecules have been omitted for clarity).

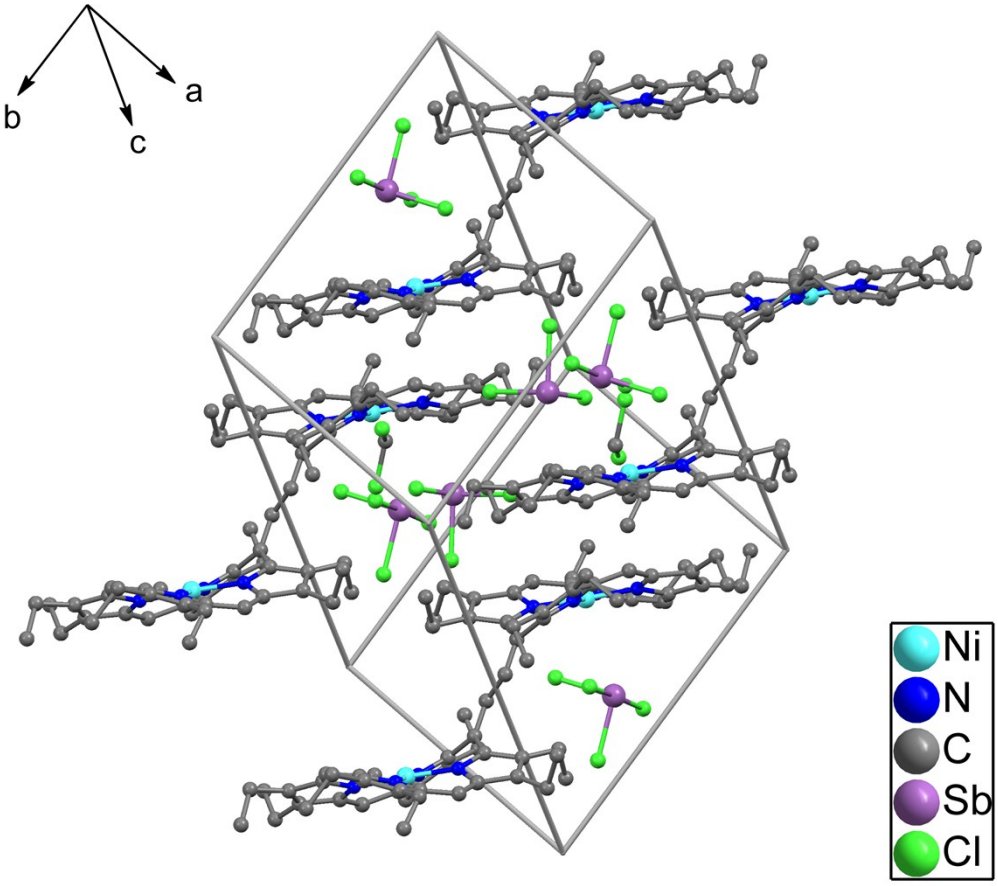

Fig. S12. Diagram illustrating the molecular packing of *P*'-[*trans*-**3**]$(SbCl_4)_2$•$2SbCl_3$•$2CH_2Cl_2$ in the unit cell (H atoms have been omitted for clarity).

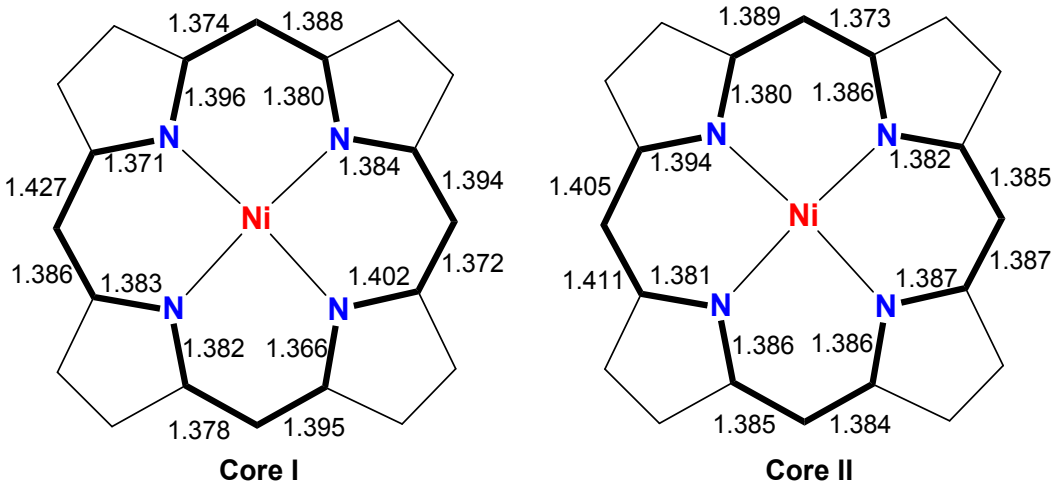

Fig. S13. Formal diagrams of the porphinato core displaying the values of the individual bond distances (in Å) in the inner 16-membered rings (bold lines) of *trans*-**1**.

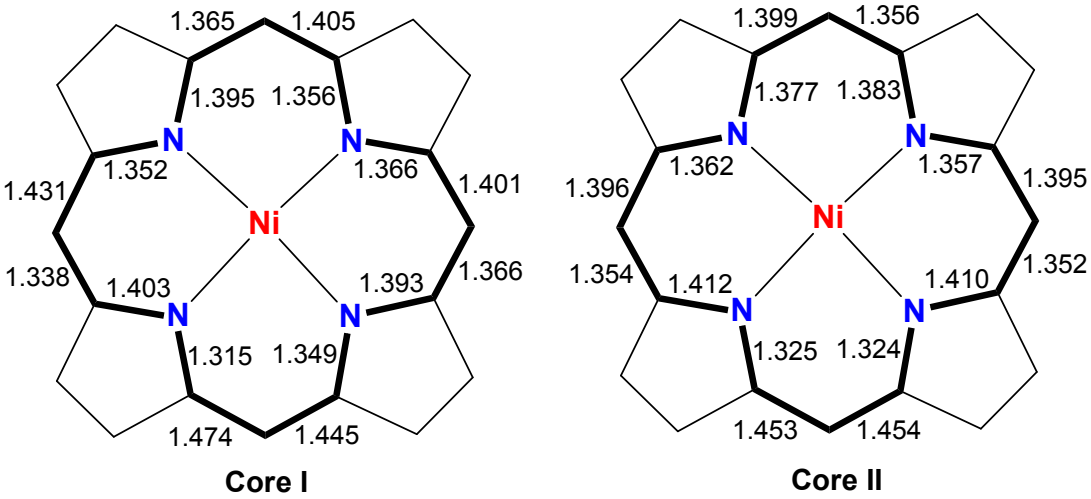

Fig. S14. Formal diagrams of the porphinato core displaying the values of the individual bond distances (in Å) in the inner 16-membered rings (bold lines) of *U*-[*trans*-**2**]$(SbCl_6)_2$. Highlight is the alternating long-short pattern of the N–C_{alpha} and C_{alpha}–C_{meso} bond distances.

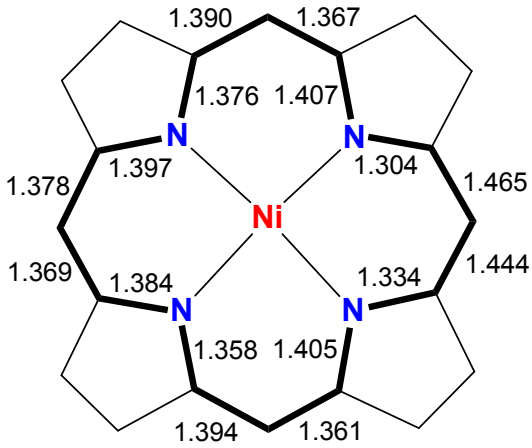

Fig. S15. Formal diagram of the porphinato core displaying the values of the individual bond distances (in Å) in the inner 16-membered rings (bold lines) of *P*'-[*trans*-**3**]$(SbCl_4)_2$•$2SbCl_3$. Highlight is the alternating long-short pattern of the N−C_{alpha} and C_{alpha}−C_{meso} bond distances.

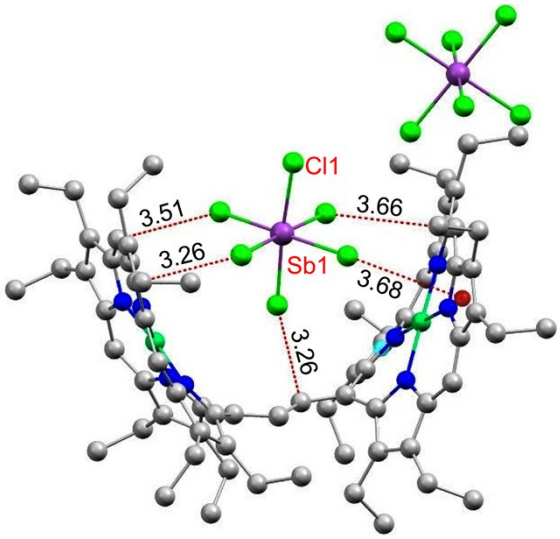

Fig . S16. X-ray crystallographic structure of *U*-[*trans*-**2**]$(SbCl_6)_2$ molecule showing anions above and below the porphyrin rings. Red dotted line: [C···Cl] short contacts in Å (hydrogen atoms are omitted for clarity).

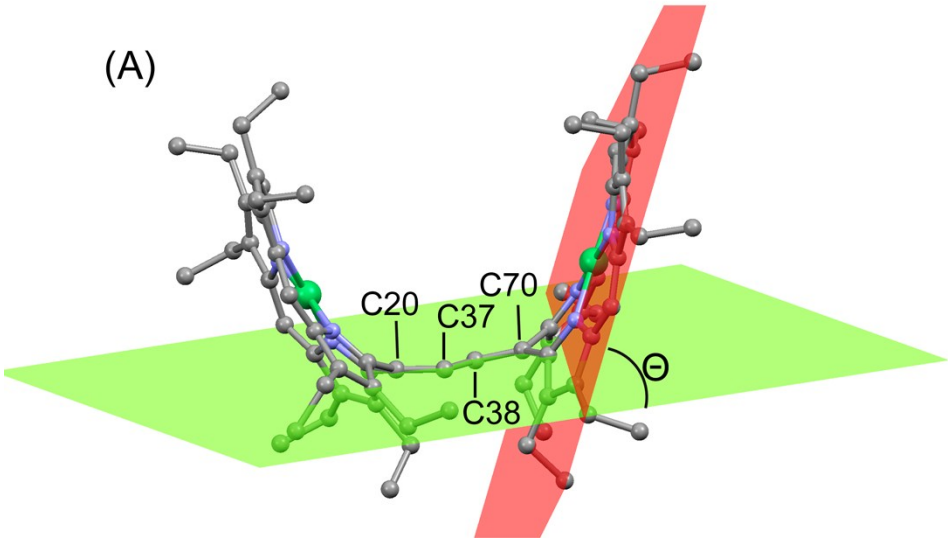

Fig. S17. Diagram illustrating the angle Θ between the least-squares plane of $C_{20}N_4$ porphyrinato core (red) and the calculated C_4 plane of the bridging ethylene group (green) of *U*-[*trans*-**2**]$(SbCl_6)_2$ as a representative case.

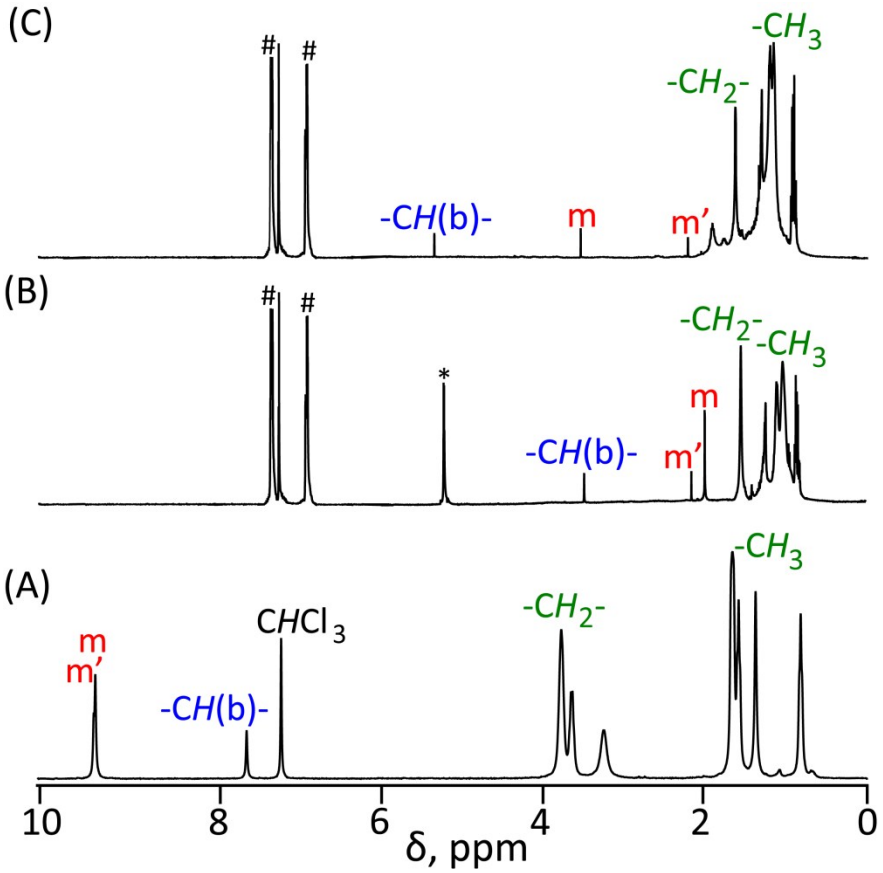

Fig. S18. ^{1}H NMR spectra of (A) *trans*-**1**, (B) *U*-[*trans*-**2**]$(SbCl_6)_2$, and (C) *P*'-[*trans*-**3**]$(SbCl_4)_2$•2$SbCl_3$ at 295 K in $CDCl_3$. Peaks marked as * and # correspond to signals from the solvent and neutral oxidant only.

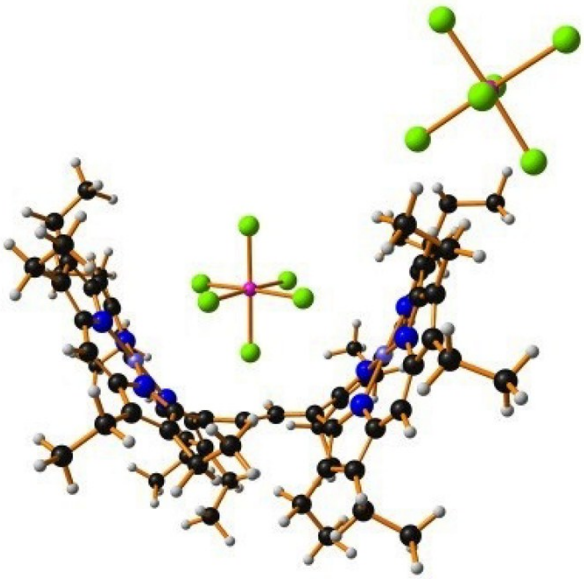

Ni-N $_{por}$ = 1.943 [1.948]
C20-C37 = 1.377 [1.406]
C37-C38 = 1.436 [1.386]
ΔG_{TS} = 8.98

U-[*trans*-^{1}**2**](SbCl$_6$)$_2$ *U*-[*trans*-^{3}**2**](SbCl$_6$)$_2$

Fig. S19. uB3LYP optimized geometry of *U*-[*trans*-**2**](SbCl$_6$)$_2$ with bond lengths in Å as calculated using cc-pVQZ basis set for Nickel atom, LANL2DZ for Sb atom and 6-31G+(d,p) for all other atoms. ΔG_{TS} is given relative to singlet spin state in kcal mol^{-1} (including ZPE).

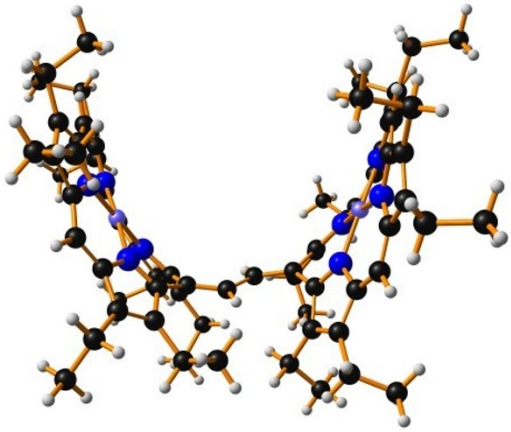

Ni-N $_{por}$ = 1.941
C20-C37 = 1.376
C37-C38 = 1.436

Fig. S20. uB3LYP optimized geometry (singlet state) of *U*-[*trans*-**2**]$^{2+}$ (without counter anion) with bond lengths in Å as calculated cc-pVQZ basis set for Nickel atom and 6-31G+(d,p) for all other atoms.

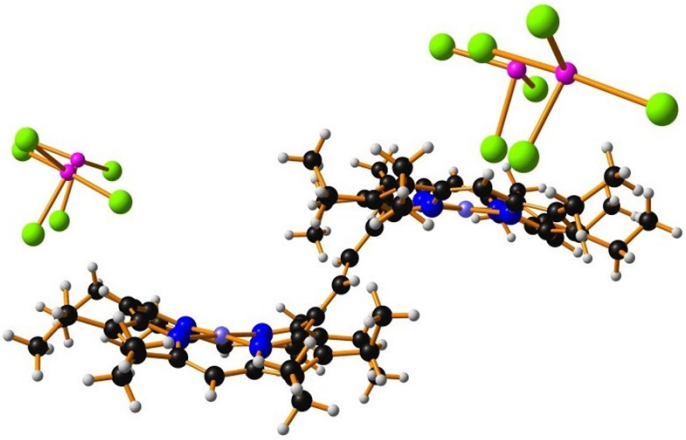

Ni-N $_{por}$ = 1.935 [1.939]
C20-C37 = 1.374 [1.402]
C37-C38 = 1.433 [1.392]
ΔG_{TS} = 6.41

P'-[*trans*-^{1}**3**](SbCl$_4$)$_2$•2SbCl$_3$ *P*'-[*trans*-^{3}**3**](SbCl$_4$)$_2$•2SbCl$_3$

Fig. S21. uB3LYP optimized geometry of *P*'-[*trans*-**3**](SbCl$_4$)$_2$•2SbCl$_3$ with bond lengths in Å as calculated using cc-pVQZ basis set for Nickel atom, LANL2DZ for Sb atom and 6-31G+(d,p) for all other atoms. ΔG_{TS} is given relative to singlet spin state in kcal mol^{-1} (including ZPE).

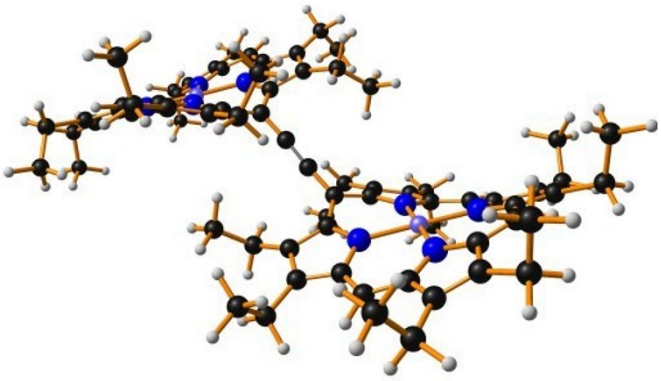

Ni-N $_{por}$ = 1.938
C20-C37 = 1.374
C37-C38 = 1.433

Fig. S22. uB3LYP optimized geometry (singlet state) of *U*-[*trans*-**2**]$^{2+}$ (without counter anion) with bond lengths in Å as calculated cc-pVQZ basis set for Nickel atom and 6-31G+(d,p) for all other atoms.

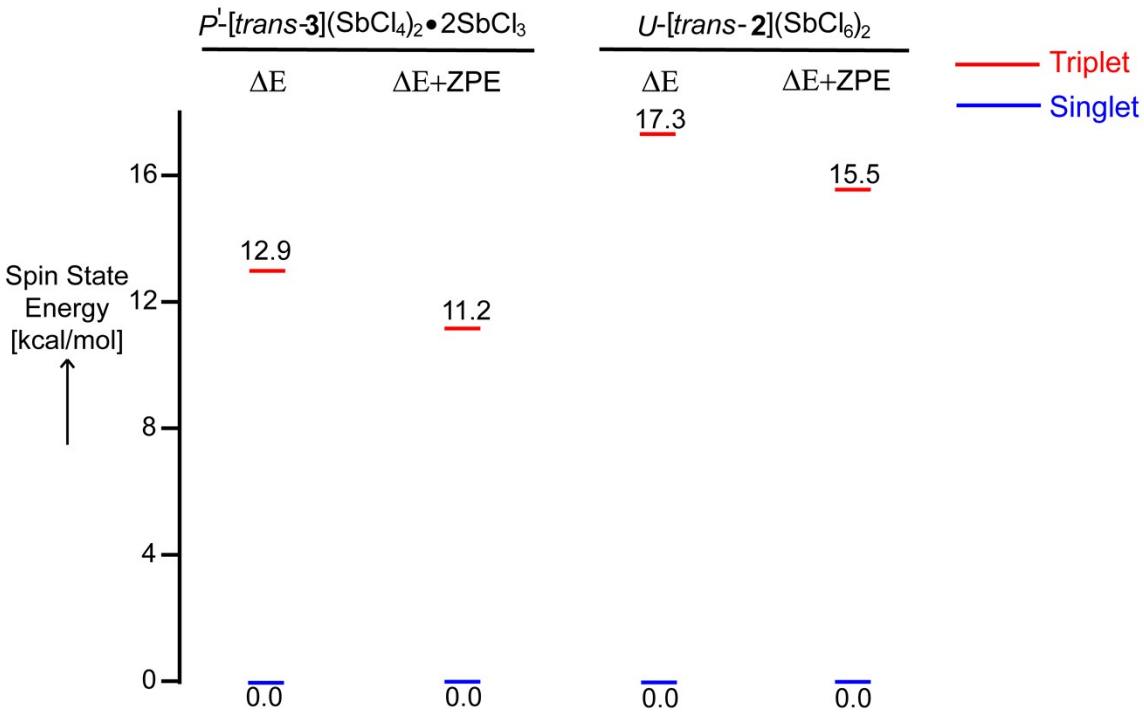

Fig. S23. Relative spin-state energies (including ZPE) of *P*'-[*trans*-^{1,3}**3**]$(SbCl_4)_2$•2$SbCl_3$ and *U*-[*trans*-^{1,3}**2**]$(SbCl_6)_2$ as calculated using uB3LYP functional in DFT. All the ΔE and ΔE+ZPE values are relative to singlet state.

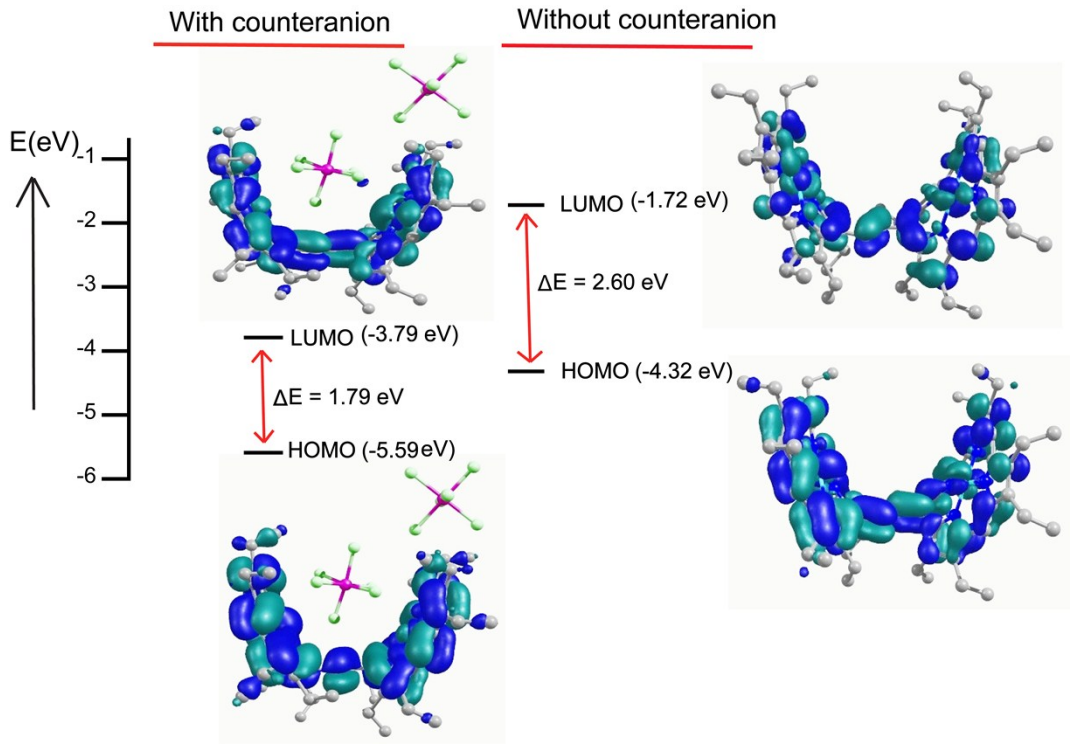

Fig. S24. Energy diagrams and selected Kohn-Sham orbitals of singlet states of *U*-[*trans*-**2**]$(SbCl_6)_2$ and *U*-[*trans*-**2**]$^{2+}$ (without counteranion) at cam- B3LYP/6-31G**/cc-pVQZ level of theory.

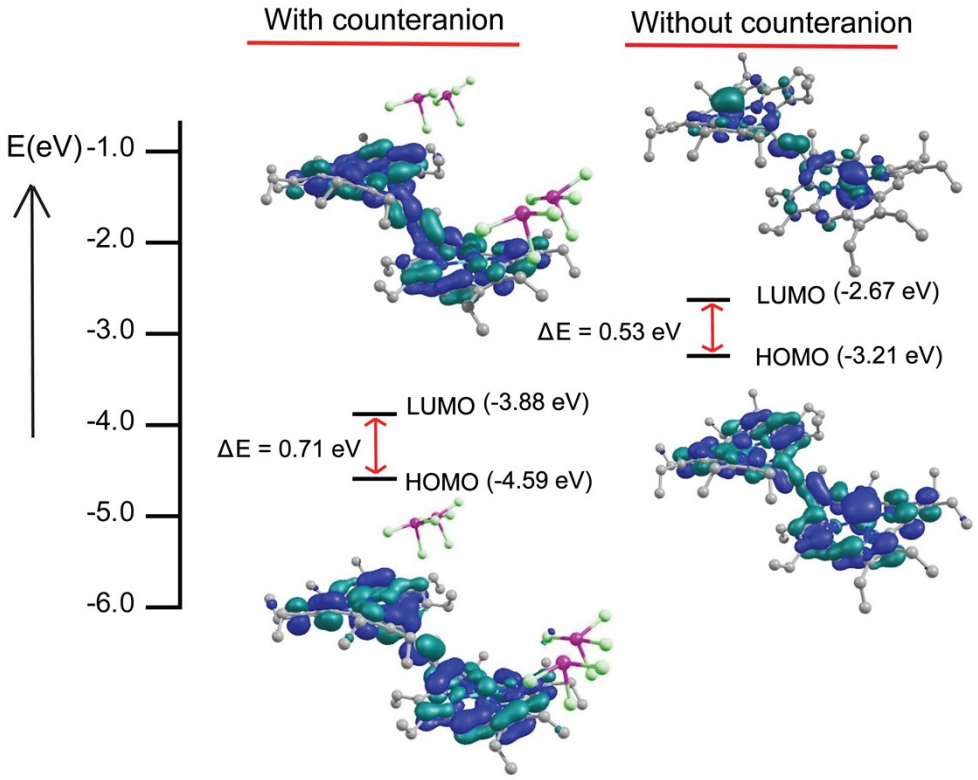

Fig. S25. Energy diagrams and selected Kohn-Sham orbitals of singlet states of *P*'-[*trans*-**3**]$(SbCl_4)_2$•$2SbCl_3$ and *P*'-[*trans*-**3**]$^{2+}$ **(**without counteranion) at cam-B3LYP/6-31G**/cc-pVQZ level of theory.

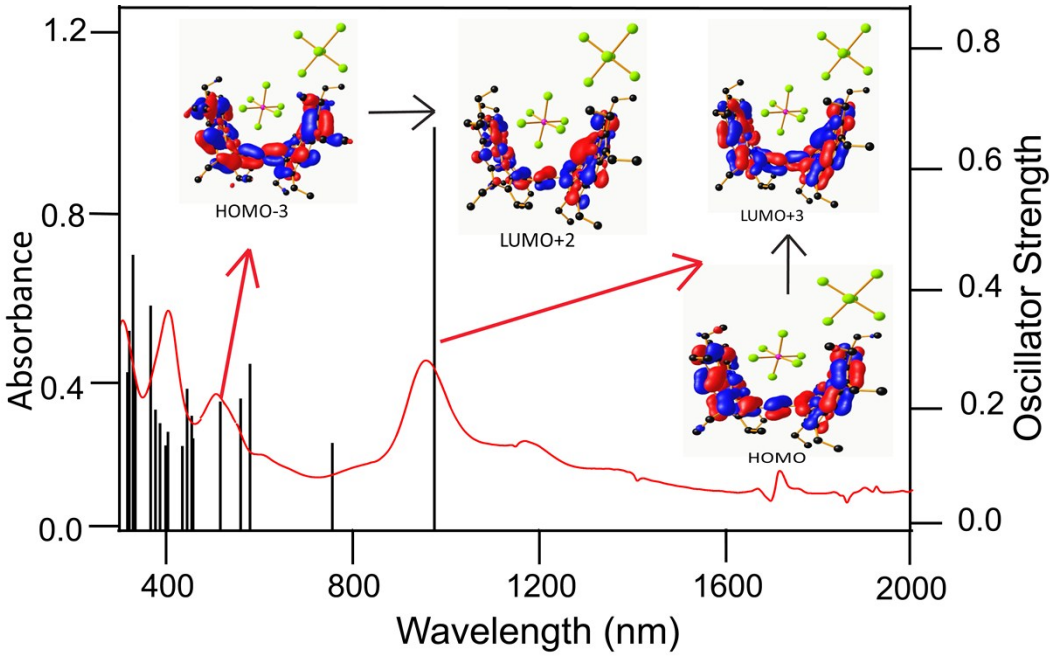

Fig. S26. Absorption spectra (curved line, left axis) of singlet state of *U*-[*trans*-**2**]$(SbCl_6)_2$ in CH_2Cl_2 and oscillator strengths (vertical line, right axis) of *U*-[*trans*-**2**]$(SbCl_6)_2$ obtained from TD-DFT calculations at the cam-B3LYP cc-pVQZ level of theory (hydrogen atoms have been omitted for clarity).

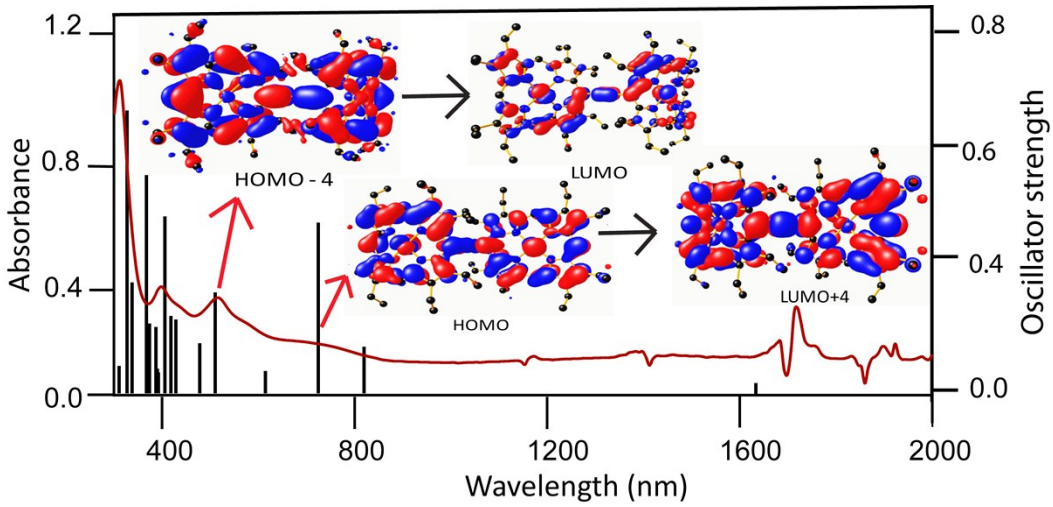

Fig. S27. Absorption spectra (curved line, left axis) of singlet state of *P*'-[*trans*-**3**]$(SbCl_4)_2$•$2SbCl_3$ in CH_2Cl_2 and oscillator strengths (vertical line, right axis) of *P*'-[*trans*-**3**]$(SbCl_4)_2$•$2SbCl_3$ obtained from TD-DFT calculations at the cam-B3LYP cc-pVQZ level of theory (hydrogen atoms and counter anions have been omitted for clarity).

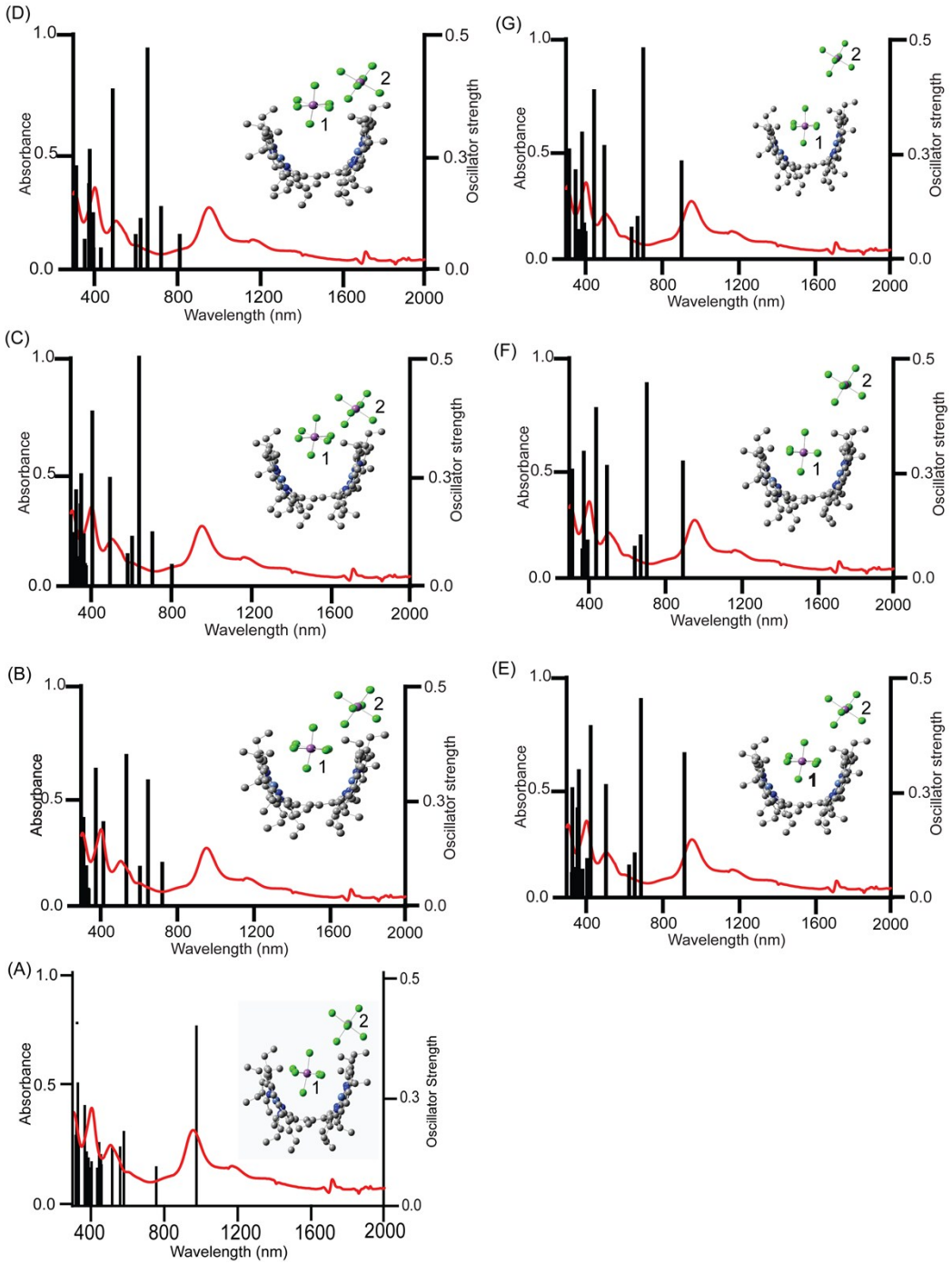

Fig. S28. Absorption spectra (curved line, left axis) of singlet state of *U*-[*trans*-**2**]$(SbCl_6)_2$ in CH_2Cl_2 and oscillator strengths obtained from TD-DFT calculations (vertical line, right axis) of (A) *U*-[*trans*-**2**]$(SbCl_6)_2$, (B-D) *U*-[*trans*-**2**]$(SbCl_6)_2$ upon stepwise shifting the counter anion 1 away from bisporphyrin cavity and (E-G) *U*-[*trans*-**2**]$(SbCl_6)_2$ upon stepwise shifting the counter anion 2 away from porphyrin ring at the cam-B3LYP cc-pVQZ level of theory.

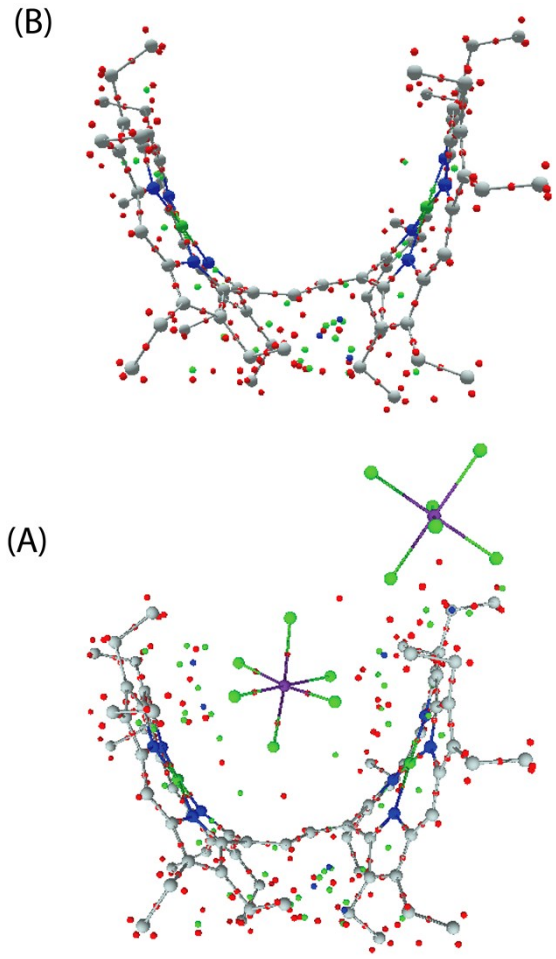

Fig. S29. DAMQT 2.1.0 picture of *U*-[*trans*-**2**]$(SbCl_6)_2$ (A) the interactions for both anions and deficient porphyrin ring are shown with top views. The blue, green and red circles represent cage (3, +3), ring (3, +1) and bond (3, -1) CPs, respectively. (B) *U*-[*trans*-**2**]$^{+2}$ (without counter anions), there are no critical points along deficient porphyrin rings.

Table S2. Crystal data and data collection parameters

	U-[*trans*-**2**](SbCl$_6$)$_2$•2CH$_2$Cl$_2$•H$_2$O	*P*'-[*trans*-**3**](SbCl$_4$)$_2$•2SbCl$_3$•2CH$_2$Cl$_2$
Formula	C76 H92 Cl16 N8 Ni2 O Sb2	C76 H92 Cl18 N8 Ni2 Sb4
T, (K)	100(2)	100(2)
Formula weight	2061.69	2360.09
Crystal system	Triclinic	Triclinic
Space group	P -1	P -1
a, Å	12.7607(11)	12.437(5)
b, Å	17.1587(15)	13.261(5)
c, Å	20.3195(17)	15.817(5)
α , deg	89.078(3)°.	65.236(5)°
β, deg	87.221(2)°.	78.258(5)°
γ, deg	82.480(2)°.	86.781(5)°
V, Å^3	4405.4(7)	2318.0(15)
Radiation (λ, Å)	Mo Kα (0.71073)	Mo Kα (0.71073)
Z	2	1
dcalcd,Mg.cm^{-3}	1.554	1.691
F(000)	2084	1170
μ, mm^{-1}	1.559	2.110
No. of unique data	16383	8596
No. of parameters, refined	1011	499
GOF on F^2	1.043	1.026
$R1$[a] [$I > 2\sigma(I)$]	0.0835	0.0580
$R1$[a] (all data)	0.1488	0.0915
wR2[b] (all data)	0.2484	0.1615

$$a\ R1 = \frac{\sum ||Fo| - |Fc||}{\sum |Fo|}; \qquad b\ wR2 = \sqrt{\frac{\sum \left[w\left(Fo^2 - Fc^2\right)^2\right]}{\sum \left[w\left(Fo^2\right)^2\right]}}$$

Table S3. Selected bond distance (Å) and angles (°).

	U-[*trans*-**2**]$(SbCl_6)_2$•$2CH_2Cl_2$•H_2O	*P*'-[*trans*-**3**]$(SbCl_4)_2$•$2SbCl_3$•$2CH_2Cl_2$
Ni(1)-N(1)	1.901(7)	1.907(5)
Ni(1)-N(3)	1.901(7)	1.887(6)
Ni(1)-N(2)	1.906(7)	1.909(6)
Ni(1)-N(4)	1.923(7)	1.906(6)
C(20)-C(37)	1.359(12)	1.358(9)
C(37)-C(38)	1.428(12)	1.416(13)
Ni(2)-N(7)	1.916(7)	-
Ni(2)-N(5)	1.914(7)	-
Ni(2)-N(6)	1.918(8)	-
Ni(2)-N(8)	1.933(8)	-
N(1)-Ni(1)-N(3)	178.8(3)	176.0(2)
N(1)-Ni(1)-N(2)	90.1(3)	90.4(2)
N(1)-Ni(1)-N(4)	88.9(3)	89.1(2)
N(2)-Ni(1)-N(4)	176.5(3)	177.8(2)
N(3)-Ni(1)-N(2)	90.7(3)	90.4(2)
N(3)-Ni(1)-N(4)	90.3(3)	89.6(3)

Table S4. TD-DFT calculated Excited States for *U*-[*trans*-**2**]$(SbCl_6)_2$.[a]

State	Energy (eV)	Wavelength (nm)	Oscillator Strength	Excitation of the main transition
11	1.2475	993.86	0.5994	HOMO ⟶ LUMO+3
14	1.6365	757.62	0.0442	HOMO-1 ⟶ LUMO+2
20	2.1360	580.44	0.1316	HOMO -3⟶ LUMO+1
22	2.2138	560.06	0.0933	HOMO ⟶ LUMO+3
24	2.3446	510.80	0.0365	HOMO-17⟶ LUMO
31	2.7015	458.05	0.0492	HOMO-9 ⟶ LUMO
32	2.7093	457.62	0.0463	HOMO-9 ⟶ LUMO
33	2.7247	455.04	0.0742	HOMO ⟶ LUMO+4
34	2.7829	445.52	0.1041	HOMO ⟶ LUMO+5
36	2.8454	435.74	0.0407	HOMO-1 ⟶ LUMO+3
47	3.0654	404.46	0.0564	HOMO-8⟶ LUMO+1
49	3.1066	399.09	0.0414	HOMO-17 ⟶ LUMO
51	3.1408	394.76	0.0654	HOMO-31⟶ LUMO
53	3.2034	387.04	387.04	HOMO-17⟶ LUMO
56	3.2803	377.37	0.1961	HOMO-1⟶ LUMO+3

[a] The states whose oscillator strengths are less than 0.03 are not included.

Table S5. TD-DFT calculated Excited States for *P*'-[*trans*-**3**]$(SbCl_4)_2$•$2SbCl_3$.[a]

State	Energy (eV)	Wavelength (nm)	Oscillator Strength	Excitation of the main transition
18	1.5312	809.73	0.7091	HOMO ⟶ LUMO
21	1.7272	717.82	0.7620	HOMO-1 ⟶ LUMO+4
22	2.0302	610.70	0.0485	HOMO-3 ⟶ LUMO
28	2.4547	505.09	0.2036	HOMO-1 ⟶ LUMO+2
33	2.5905	478.60	0.1095	HOMO-7 ⟶ LUMO
38	2.8730	431.55	0.1471	HOMO ⟶ LUMO+8
41	2.9438	421.18	0.1685	HOMO-12 ⟶ LUMO
44	3.0300	409.19	0.4430	HOMO-11 ⟶ LUMO
48	3.1303	396.08	0.0599	HOMO ⟶ LUMO+10
53	3.1709	391.05	0.1851	HOMO-16 ⟶ LUMO
55	3.2846	377.48	0.1539	HOMO-2 ⟶ LUMO+4
57	3.3377	371.47	0.0632	HOMO-3 ⟶ LUMO+4
67	3.6191	342.59	0.2756	HOMO-1 ⟶ LUMO+7

[a] The states whose oscillator strengths are less than 0.03 are not included.

Table S6: DFT/UB3LYP calculated stabilization energies (ΔE) in kcal/mol of *U*-[*trans*-**2**]$^{2+}$ and *P*'-[*trans*-**3**]$^{2+}$ (without counter anion)**.**

U-[*trans*-**2**]$^{2+}$	*P*'-[*trans*-**3**]$^{2+}$	**ΔE**
-3970084.678	-3970159.917	75.23

Table S7: DFT/UB3LYP calculated interaction energies ($\boldsymbol{E_{int}}$) in kcal/mol of *U*-[*trans*-**2**]$(SbCl_6)_2$ and *P*'-[*trans*-**3**]$(SbCl_4)_2$•$2SbCl_3$.

Complexes	**Interaction Energy (kcal/mol)**
U-[*trans*-**2**]$(SbCl_6)_2$	194.92
P'-[*trans*-**3**]$(SbCl_4)_2$•$2SbCl_3$	26.23

Table S8: The electron density (ρ) and Laplacian ($\Delta^2\rho$), the electronic potential energy density (V), the electronic kinetic energy density (G) and the electronic energy density (H) at the intermolecular bond critical (3, -1) and cage critical (3, +3) points of *U*-[*trans*-**2**]$(SbCl_6)_2$.

Atom pairs	**CPs**	$\boldsymbol{\rho(r)}$	$\boldsymbol{\Delta^2\rho}$	$\boldsymbol{V(r)}$	$\boldsymbol{G(r)}$	$\boldsymbol{H(r)}$
Cl173···H57	217	0.00131	0.00820	-0.00072	0.00138	0.00066
Cl173···C11	231	0.00343	0.01999	-0.00231	0.00365	0.00134
Cl174···Ni171	289	0.00654	0.01250	-0.00232	0.00272	0.00040
Cl174···C80	336	0.00443	0.02518	-0.00307	0.00468	0.00161
Cl175···H134	278	0.00139	0.00861	-0.00077	0.00146	0.00069
Cl175···C93	324	0.00532	0.03042	-0.00364	0.00562	0.00198
Cl176···Cl182	241	0.00270	0.01844	-0.00199	0.00330	0.00130
Cl176···H58	212	0.00035	0.00274	-0.00021	0.00045	0.00023
Cl177···H64	223	0.00152	0.00947	-0.00093	0.00165	0.00071
Cl177···H58	211	0.00226	0.01345	-0.00137	0.00236	0.00099
Cl177···C13	228	0.00424	0.02581	-0.00310	0.00478	0.00167
Cl178···H169	345	0.00186	0.01352	-0.00141	0.00239	0.00098
Cage Critical Points	224	0.00048	0.00425	-0.00034	0.00070	0.00036
	245	0.00049	0.00364	-0.00027	0.00059	0.00031
	397	0.00210	0.01196	-0.00133	0.00216	0.00082
	286	0.00024	0.00233	-0.00016	0.00037	0.00021

Table S9: The electron density (ρ) and Laplacian ($\Delta^2\rho$), the electronic potential energy density (*V*), the electronic kinetic energy density (*G*) and the electronic energy density (*H*) at the intermolecular bond critical (3, -1) points of *P*'-[*trans*-**3**]$(SbCl_4)_2$•$2SbCl_3$.

Atom pairs	**CPs**	***ρ(r)***	***Δ²ρ***	***V(r)***	***G(r)***	***H(r)***
Cl2···H82	260	0.00214	0.01285	-0.00123	0.00222	0.00098
Cl3···H82	254	0.00325	0.01929	-0.00209	0.00345	0.00136
Cl3···H75	274	0.00122	0.00762	-0.00065	0.00128	0.00062
Cl4···H32	313	0.00342	0.01949	-0.00203	0.00345	0.00142
Cl4···H75	305	0.00326	0.01907	-0.00206	0.00341	0.00135
Cl4···H78	326	0.00458	0.02564	-0.00292	0.00467	0.00174
Sb1···Cl17	217	0.02060	0.05366	-0.01170	0.01256	0.00085
Cl189···H152	268	0.00533	0.02921	-0.00340	0.00535	0.00194
Cl189···H146	220	0.00192	0.01153	-0.00107	0.00197	0.00090
Cl189···C111	243	0.00313	0.01805	-0.00180	0.00316	0.00135
Cl184···H153	337	0.00494	0.02735	-0.00315	0.00499	0.00184